NJC

Accepted Manuscript

This article can be cited before page numbers have been issued, to do this please use: M. R. Maurya, B. Mengesha, B. Uprety, N. Jangra, R. Tomar and F. Avecilla, *New J. Chem.*, 2018, DOI: 10.1039/C7NJ03551A.

View Article Online
DOI: 10.1039/C7NJ03551A

Oxygen atom transfer between DMSO and benzoin catalyzed by *cis*–dioxidomolybdenum(VI) complexes of tetradentate Mannich Bases†

Mannar R. Maurya, *[a] Bekele Mengesha,[a] Bhawna Uprety,[a] Nancy Jangra,[a] Reshu Tomar[a] and Fernando Avecilla[b]

[a]*Department of Chemistry, Indian Institute of Technology Roorkee, Roorkee–247667, India. E–mail: rkmanfcy@iitr.ac.in; Fax: +91 1332 273560; Tel: +91 1332 285327*

https://www.iitr.ac.in/CY/rkmanfcy

[b]*Grupo Xenomar, Centro de Investigacións Científicas Avanzadas (CICA), Departamento de Química, Facultade de Ciencias, Universidade da Coruña, Campus de A Coruña, 15071 A Coruña, Spain*

† Electronic supplementary information (ESI) available: Figs. S1–S4 contain crystal packing of complexes **1**, **2**, **3** and **5**. Figs. S5 – S12 contain ^{1}H NMR spectra of ligands and complexes. Fig. S13 and Table S1present catalytic results for 4-chlorobenzene. CCDC 1573125 (for **1**), 1573126 (for **2**), 1573127 (for **3**) and 1573128 (for **5**) contain the supplementary crystallographic data. For ESI and crystallographic data in CIF or other electronic format see DOI: xxxxxxxx

<<Abstract>>

The reaction of dibasic tetradentate ONNO donor Mannich bases derived from ethylenediamine and 2,4–di–*tert*–butylphenol (H_2L^1), 2,4–di–methylphenol (H_2L^2), 2–*tert*–butyl–4–methylphenol (H_2L^3), 2,4–di–chlorophenol (H_2L^4) and 2-naphthol (H_2L^5) with [$Mo^{VI}O_2(acac)_2$] (Hacac = acetylacetone) in a 1:1 molar ratio in refluxing MeOH gave the corresponding *cis*-dioxidomolybdenum(VI) complexes [$Mo^{VI}O_2(L^1)$], [$Mo^{VI}O_2(L^2)$], [$Mo^{VI}O_2(L^3)$], [$Mo^{VI}O_2(L^4)$], and [$Mo^{VI}O_2(L^5)$], respectively. All complexes were characterized by elemental analysis, various spectroscopic (FT-IR, UV/Vis, ^{1}H and^{13}C NMR) techniques and single-crystal X-ray analysis (of **1**, **2**, **3** and **5**). These complexes adopt a distorted six-coordinated octahedral geometry where ligands act as tetradentate, coordinating through the two $O_{phenolate}$ and two N_{amine} atoms in a cis-α type binding mode involving coordination of one of the N_{amine} atom in the apical position and one O_{oxido} terminal oxygen atom in the equatorial position. These complexes catalyze oxygen atom transfer between benzoin and dimethyl sulfoxide (DMSO) in acetonitrile at 80 °C. The formation

View Article Online
DOI: 10.1039/C7NJ03551A

of benzil could easily be monitored by HPLC. The electronic effect caused by the *para* substituent and the steric effect caused by the *ortho* substituent influence the formation of benzil and therefore conversion varied between 68 - 99% in 18 h of reaction time under optimized conditions; most active catalyst being $[Mo^{VI}O_2(L^5)]$. Almost similar trend has also been obtained with 4-chlorobenzoin. The pseudo first order rate constant for $[Mo^{VI}O_2(L^5)]$ was found to be 0.0998 h^{-1}. During catalytic reaction, the formation of the binuclear intermediate and its fast decay into the initial dioxidomolybdenum(VI) complex was established by time dependent UV/Vis studies.

Introduction

The most prominent role of second row transition element, molybdenum, in chemistry and biology is that of an important bio–catalyst, since a wide variety of chemical transformations in biology are catalyzed by molybdenum enzymes.[1] Molybdenum enzymes have long enjoyed the status of being vital eukaryotic enzymes catalyzing reactions involved in carbon, nitrogen and sulfur bio geochemical cycles in the atmosphere.[2] Apart from nitrogenases (in which the metal is incorporated into a unique $[MoFe_7S_9]$ cluster) all molybdenum enzymes are quite uniform in their active site structure and can be divided into three large and non–overlapping families, as exemplified by the enzymes xanthine oxidase, sulfite oxidase and DMSO reductase.[3,4] In all of these families, the molybdenum cofactor (commonly abbreviated as Moco), consists of a molybdenum ion coordinated to either one or two bidentate pterindithiolene ligands ([2–amino–4(1*H*)–pteridinone]).[3,5] The enzymes from the DMSO reductase family (the most diverse of all) have only been found in bacteria and archea whilst enzymes from the other two families are found in all forms of life.[6,7]

The DMSO reductase family is the largest family of molybdopterin enzymes, and is widely studied for its reactivity and mechanism. They oxidize or reduce suitable substrates (for e.g. DMSO to DMS), and thus catalyze oxygen atom transfer (OAT) reactions according to equation 1.[2b] The process is accompanied by two electron reduction, and usually the oxygen removed from the substrate (SO) coordinates the metal in the oxidized state. Thus, the presence of Mo=O moiety become an essential functional requirement for model studies for this class of enzymes.[6,8,9]

$$[Mo^{VI}O_n]^{2+} + S \rightleftharpoons [Mo^{IV}O_{n-1}]^{2+} + SO \quad n = 1,2 \quad (1)$$

View Article Online
DOI: 10.1039/C7NJ03551A

One of the most explored enzymes of DMSO reductase family is the name enzyme, DMSO reductases. It catalyses the reduction of DMSO to DMS, and the molybdenum center shuttles between Mo(VI) and Mo(IV) oxidation states during the catalytic cycle. A number of structurally diverse dioxidomolybdneum(VI) complexes have been developed and evaluated for their oxygen atom transfer abilities for biomimetic modelling as well as industry relevant processes.[10-13] Most of these model studies are based on oxygen atom transfer involving tertiary phosphines and/or DMSO. Tertiary phosphines are not the biological substrate for DMSO reductases, however, they are often a substrate of choice for OAT modelling studies, since their properties can be desirably tuned and the reactions can be easily monitored by ^{31}P NMR studies.[13-20]

In our recent reports, we have evaluated the OAT ability of *cis*–dioxidomolybdenum(VI) complexes built on aminobisphenoltripodal ligands,[21] between DMSO and benzoin in acetonitrile at 80 ^{o}C in 24 h of reaction time. Similar reactions have also been reported by Sillanpää *et al.* and Ng *et al.* in DMSO at ambient temperature.[22-24] A detailed mechanistic study had revealed an overall steric control in our reactions.[21] We have further extended the study to a new series of *cis*–$[MoO_2]^{2+}$ complexes derived from Mannich bases of ethylenediamine and 2,4–disubstituted phenols. The present systems employed for catalytic OAT reactions were made sterically less hindered by using dipodal ligands, as against tripodal ligands reported earlier by us. We have achieved almost 99 % conversion in only 18 h of reaction time. We have also derived the second order rate equation using the most active catalyst, $[MoO_2L^5]$.

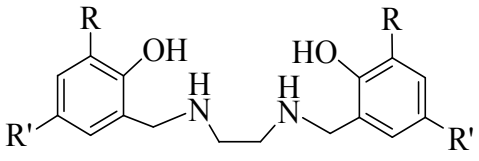

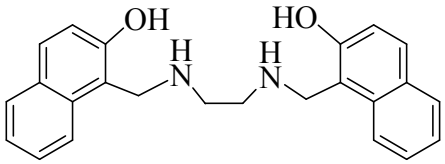

R	R'	Ligand	H_2L^5 **V**
tert–butyl	*tert*–butyl	H_2L^1 **I**	
Methyl	Methyl	H_2L^2 **II**	
tert–butyl	Methyl	H_2L^3 **III**	
Chloro	Chloro	H_2L^4 **IV**	

Scheme 1 Structure of ligands used in this study.

View Article Online
DOI: 10.1039/C7NJ03551A

Experimental Section

Materials and general methods

Ammonium molybdate, acetylacetone (SRL, India), 2,4–di–*tert*–butylphenol, 2,4–di–methylphenol, 2–*tert*–butyl–4–methylphenol, 2,4–di–chlorophenol, ethylenediammine (Himedia, India), benzoin (S.D. fine chemicals, India), formaldehyde and DMSO (Rankem, India) were used as obtained. Other chemicals and solvents were of AR grade. The precursor complex $[Mo^{VI}O_2(acac)_2]$ was prepared following a literature method.[25]

All measurements were made after drying the metal complexes at 100 ˚C. Elemental analyses of the complexes were carried out on an Elementar model Vario–EI–III after drying the samples at 100 °C. IR spectra were recorded as KBr pellets on a Nicolet 1100 FT–IR spectrometer. Electronic spectra of the complexes were recorded in acetonitrile on a Shimadzu 1601 UV–Vis spectrophotometer. ^{1}H and ^{13}C NMR spectra were recorded in $CDCl_3$/DMSO-d_6 on a JEOL ECX 400 MHz spectrometer. GC–MS was run on a Perkin–Elmer Clarus 500 instrument. HPLC was performed on a Shimadzu LC–2010A HT instrument using 250 × 4.6 mm C-18 column in low pressure gradient mode with a flow rate of 0.5 mL min^{-1} and injection volume of 40 µL. The mobile phase used was MeCN : H_2O : trifluoroacetic acid, 60 : 40 : 0.02.

Preparation of ligands

H_2L^1 I. A solution of ethylenediammine (0.300 g, 5 mmol), 39% formaldehyde (0.770 g, 10 mmol,) and 2,4−di−*tert*−butylphenol (2.063 g, 10 mmol) in MeOH (20 mL) was refluxed for ca. 18 h. During this period, a white solid slowly separated; the solid was collected by filtration, washed well with cold MeOH and then dried under vacuum. Yield: 1.90 g (76%). (Found: C 76.69; H, 10.35; N, 5.70%. Calcd for $C_{32}H_{52}N_2O_2$ (496.0 g mol^{-1}): C, 77.37; H, 10.55; N, 5.64%). ^{1}H NMR (400 MHz, $CDCl_3$): δ 10.73 (br, 2H, OH), 7.25 (s, 2H), 6.85 (s, 2H) (aromatic), 3.92 (s, 4H, -CH_2-), 3.54 (s, 2H, -NH), 3.03 (s, 4H, -CH_2CH_2-), 1.44 (s, 18H), 1.30 (s, 18H, -CH_3). ^{13}C NMR (400 MHz, $CDCl_3$): δ 150.83, 142.17, 136.68, 121.87, 118.89, 82.23, 51.35, 49.69, 34.89, 34.27, 31.58, 29.61.

Ligands H_2L^2 **II**, H_2L^3 **III**, H_2L^4 **IV** and H_2L^5 **V** were prepared by the procedure outlined for H_2**L^1** using 10 mmol each of 2,4-di-methylphenol, 2–*tert*–butyl–4–methylphenol, 2,4–di–chlorophenol and 2-naphtol, respectively, in place of 2-tert-butyl-4-methylphenol.

View Article Online
DOI: 10.1039/C7NJ03551A

H_2L^2 II. Yield: 1.22 g (74%). (Found: C, 73.46; H, 8.42; N, 8.81%. Calcd for $C_{20}H_{28}N_2O_2$ (328.0g mol^{-1}): C, 73.14; H, 8.59; N, 8.53%. ^1H NMR (400 MHz, $CDCl_3$): δ 10.42 (br, 2H, OH), 6.89 (s, 2H), 6.66 (s, 2H) (aromatic), 3.85 (s, 4H, -CH_2-), 3.54 (s, 2H, -NH), 2.97 (s, 4H, -CH_2CH_2-), 2.22 (s, 12H, -CH_3). ^{13}C NMR (400 MHz, $CDCl_3$): δ 153.13, 131.24, 127.86, 126.29, 124.88, 120.61, 58.36, 51.77, 20.46, 15.86.

H_2L^3 III. Yield: 1.04 g (50%). (Found: C, 75.17; H, 9.54; N, 6.90%. Calcd for $C_{26}H_{40}N_2O_2$ (412.0 g mol^{-1}): C, 75.68; H, 9.77; N, 6.79%. ^1H NMR (400 MHz, $CDCl_3$): δ 10.58 (br, 2H, OH), 6.98 (s, 2H), 6.66 (s, 2H) (aromatic), 3.85 (s, 4H, -CH_2-), 3.44 (s, 2H, -NH), 2.99 (s, 4H, -CH_2CH_2-), 2.22 (s, 6H), 1.41 (s, 18H) (CH_3). ^{13}C NMR (400 MHz, $CDCl_3$): δ 154.21, 136.07, 127.47, 126.83, 121.78, 100.03, 58.05, 50.89, 34.48, 29.89, 20.64.

H_2L^4 IV. Yield: 1.28 g (62%). (Found: C, 48.44; H, 4.06; N, 6.92%. Calcd for $C_{16}H_{16}N_2O_2Cl_4$ (410.12 g mol^{-1}): C, 46.86; H, 3.93; N, 6.83%. ^1H NMR (400 MHz, $CDCl_3$): δ 7.34 (s, 2H), 7.07 (s, 2H) (aromatic), 3.97 (s, 4H, -CH_2-), 4.96 (s, 2H, -NH), 2.79 (s, 4H, -CH_2CH_2-). ^{13}C NMR (400 MHz, DMSO-d_6): δ 154.26, 127.92, 127.33, 126.84, 121.33, 121.18, 50.71, 46.48.

H_2L^5 V. Yield: 1.02 g (55%). (Found: C, 73.86; H, 6.61; N, 7.73%. Calcd for $C_{24}H_{24}N_2O_2$ (372.46 g mol^{-1}): C, 77.39; H, 6.49; N, 7.52%).^1H NMR (400 MHz, d_6-[DMSO]): δ 6.12 (d, 2H), 7.12 (d, 2H), 7.26 (dd, 2H), 7.68 (dd, 2H), 7.71 (d, 2H), 7.98 (d, 2H), (aromatic), 4.74 (s, 4H -CH_2-), 5.00 (s, 2H, -NH), 4.07 (s, 4H -CH_2CH_2-).

Preparations of complexes

$[MoO_2L^1]$ 1. To a suspension of H_2L^1 (0.496 g, 1.0 mmol) in MeOH (10 mL) was added a filtered solution of metal precursor [$Mo^{VI}O_2(acac)_2$] (0.326 g, 1.0 mmol) in MeOH (10 mL) with magnetic stirring where a clear orange solution was obtained within a few minutes. The resulting reaction mixture was then heated under reflux for 4 h on a water bath. After cooling to room temperature, the precipitated orange solid was collected by filtration, washed with cold MeOH and dried under vacuum. Yield 0.461 g (74%). (Found: C, 61.36; H, 8.24; N, 4.58%. Calcd for $C_{32}H_{50}N_2O_4Mo$ (622.0 g mol^{-1}): C, 61.72; H, 8.09; N, 4.50%). ^1H NMR (400 MHz, $CDCl_3$): δ 7.26 (s, 2H), 6.86 (s, 2H) (aromatic), 5.17-5.18 (d, 1H), 5.20-5.21 (d, 1H), 3.93-3.94 (d, 1H),

View Article Online
DOI: 10.1039/C7NJ03551A

3.97-3.98 (d, 1H) (-CH_2-), 2.94 (s, 2H, -NH), 2.68-2.73 (t, 2H), 2.84-2.87 (t, 2H) (-CH_2CH_2-), 1.43 (s, 18H), 1.28 (s, 18H) (-CH_3). ^{13}C NMR (400 MHz, $CDCl_3$): δ 154.23, 140.84, 135.83, 123.43, 123.20, 120.97, 59.34, 51.87, 35.01, 34.28, 31.80, 29.75.

Complexes **2**–**5** were prepared similarly using [$Mo^{VI}O_2(acac)_2$] (0.326 g, 1.0 mmol) and respective ligands (1.0 mmol).

[MoO_2L^2] 2. Yield 0.363 g (80%). (Found: C, 75.17; H, 9.54; N 6.90%. Calcd for $C_{20}H_{26}N_2O_4Mo$ (454.0 g mol^{-1}): C, 52.86; H, 5.77; N 6.17%). ^{1}H NMR (400 MHz, $CDCl_3$): δ 6.68 (s, 2H), 6.89 (s, 2H) (aromatic), 5.21-5.24 (d, 2H), 3.94-3.96 (d, 2H) (-CH_2-), 2.70 (s, 2H, -NH), 3.05 (s, 2H), 2.91 (s, 2H) (-CH_2CH_2-), 2.23 (s, 6H), 2.19 (s, 6H) (CH_3). ^{13}C NMR (400 MHz, $CDCl_3$): δ 156.36, 137.86, 130.45, 129.47, 119.56, 99.81, 53.45, 45.49, 20.52, 17.03.

[MoO_2L^3] 3. Yield 0.480 g (89 %). (Found: C, 57.47; H, 7.23; N, 5.41%. Calcd for $C_{26}H_{38}N_2O_4Mo$ (538.0 g mol^{-1}): C, 57.98; H, 7.11; N, 5.20%). ^{1}H NMR (400 MHz, $CDCl_3$): δ 6.89 (s, 2H), 6.68 (s, 2H) (aromatic), 5.21 (d, 1H), 5.24 (d, 2H), 3.95 (d, 1H), 3.97 (d, 1H) (-CH_2-), 2.91 (s, 2H, -NH), 3.05-3.08 (t, 2H), 2.70-2.73 (t, 2H) (-CH_2CH_2-), 2.27 (s, 6H), 1.58 (s, 18H) (CH_3). ^{13}C NMR (400 MHz, $CDCl_3$): δ 156.71, 138.5, 129.18, 126.71, 127.77, 121.23, 53.20, 45.71, 34.58, 29.36, 20.60.

[MoO_2L^4] 4. Yield 0.487 g (91%). (Found: C, 35.59; H, 2.54; N, 5.29%. Calcd for $C_{16}H_{14}Cl_4N_2O_4Mo$ (536.0 g mol^{-1}): C, 35.85; H, 2.63; N 5.23%). ^{1}H NMR (400 MHz, DMSO): δ 7.20 (s, 2H), 7.40 (s, 2H) (aromatic), 4.72 (dd, 2H), 3.95 (dd, 2H) (-CH_2-), 5.40 (s, 2H, -NH), 2.17 (t, 2H), 2.80-2.76 (t, 2H) (-CH_2CH_2-). ^{13}C NMR (400 MHz, DMSO-d_6): δ 154.43, 128.17, 127.53, 125.42, 123.36), 123.04, 52.31, 45.72.

[MoO_2L^5] 5. Yield 0.417 g (83%). (Found: C, 58.23; H, 4.54; N, 5.47%. Calcd for $C_{24}H_{22}N_2O_4Mo$ (498.0 g mol^{-1}): C, 57.84; H, 4.45; N 5.62%). ^{1}H NMR (400 MHz, $CDCl_3$): δ 7.00 (d, 2H), 7.40 (d, 2H), 7.62 (dd, 2H), 7.75 (dd, 2H), 7.86 (d, 2H), 7.98 (d, 2H), (aromatic), 3.09 (dd, 2H), 4.40 (dd, 2H) (-CH_2-), 5.00 (s, 2H, -NH), 1.27 (t, 2H), 1.75 (t, 2H) (-CH_2CH_2-).

View Article Online
DOI: 10.1039/C7NJ03551A

X-Ray crystal structure determination

Three-dimensional X-ray data were collected on a Bruker Kappa Apex CCD diffractometer at low temperature for **2** and at room temperature for **1**, **3** and **5**, by the ϕ-ω scan method. Reflections were measured from a hemisphere of data collected from frames, each of them covering 0.3º in ω. A total of 78032 for **1**, 47390 for **2**, 64461 for **3** and 36101 for **5** reflections measured were corrected for Lorentz and polarization effects and for absorption by multi-scan methods based on symmetry-equivalent and repeated reflections. A total of 5937 for **1**, 4529 for **2**, 3886 for **3** and 3813 for **5**, independent reflections exceeded the significance level ($|F|/\sigma|F|$) > 4.0, respectively. After data collection, in each case an empirical absorption correction (SADABS)[26] was applied, and the structures were solved by direct methods and refined by full matrix lea st-squares on F^2 data using SHELX suite of programs.[27] In **1**, hydrogen atoms were included in calculated position and refined in the riding mode, except for N(1) and N(2), which were located in difference Fourier map and fixed to the nitrogen atoms. In **2** and **3**, hydrogen atoms were located in difference Fourier map and left to refine freely, except for C(2), C(10), C(11), C(19) and C(20) in **2**, and C(8), C(9), C(10), C(11), C(23), C(24), C(25) and C(26) in **3**, which were included in calculated position and refined in the riding mode, respectively. In **5**, hydrogen atoms were included in calculated position and refined in the riding mode, except for C(8), N(1) and N(2), which were located in difference Fourier map and left to refine freely. Refinements were done with allowance for thermal anisotropy of all non-hydrogen atoms. A final difference Fourier map showed no residual density outside, except for compound **1**, due to a disordered water molecules which were not refined: 1.369 and -0.524 e.Å^{-3} for **1**, 0.411 and -0.318 for **2** and 0.605 and -0.588 e.Å^{-3} for **3** and 0.569 and -0.735 for **5**. A weighting scheme w = $1/[\sigma^2(F_o^2) + (0.108000\ P)^2 + 2.394000\ P]$ for **1**, w = $1/[\sigma^2(F_o^2) + (0.024300\ P)^2 + 1.332900\ P]$ for **2,** , w = $1/[\sigma^2(F_o^2) + (0.054500\ P)^2 + 0.00000\ P]$ for **3** and w = $1/[\sigma^2(F_o^2) + (0.066700\ P)^2 + 0.00000\ P]$ for **5**, where P = $(|F_o|^2 + 2|F_c|^2)/3$, were used in the latter stages of refinement. An important disorder on *t*-butyl groups appear in the crystal of **1**. This disorder has been refined and two atomic sites have been observed and refined with the anisotropic atomic displacement parameters for two *t*-butyl groups. More specifically this disorder was refined using 243 restraints (ISOR, SADI, SIMU and DELU restraints were used). The site occupancy factors were 0.43339 for C(15A), C(16A) and C(17A) and 0.45583 for C26(A), C(27A) and C(28A). Further details of the crystal structure determination are given in Table 1.

View Article Online
DOI: 10.1039/C7NJ03551A

Table 1 Crystal data and structure refinement for $[MoO_2(L^1)]$ **1**, $[MoO_2L^2]$ **2**, $[MoO_2(L^3)]$ **3** and $[MoO_2(L^5)]$ **5**. . CCDC: 1573125-1573128.

	1	**2**	**3**	**5**
Formula	$C_{32}H_{50}MoN_2O_4$	$C_{20}H_{26}MoN_2O_4$	$C_{26}H_{38}MoN_2O_4$	$C_{24}H_{22}MoN_2O_4$
Formula weight	622.68	454.37	538.52	498.38
T, *K*	293(2)	99(2)	293(2)	296(2)
Wavelength, Å	0.71073	0.71073	0.71073	0.71073
Crystal system	Trigonal	Monoclinic	Orthorhombic	Monoclinic
Space group	$P\bar{3}$	$P2_1/c$	Pcab	$P2_1/c$
a/Å	19.0694(6)	12.1153(11)	12.9405(4)	15.164(2)
b/Å		10.9427(10)	14.0380(4)	12.8563(18)
c/Å	17.1332(6)	15.7160(14)	28.3268(10)	10.6927(14)
α/º	90	90	90	90
β/º	90	112.296(4)	90	90.963(7)
γ/º	120	90	90	90
V/Å^3	5395.6(3)	1927.8(3)	5145.8(3)	2084.2(5)
Z	6	4	8	4
F_{000}	1980	936	2256	1016
D_{calc}/g cm^{-3}	1.150	1.566	1.390	1.588
μ/mm^{-1}	0.397	0.709	0.543	0.664
θ/ (º)	1.19 to 28.28	1.82 to 28.32	1.44 to 28.40	1.34 to 28.37
R_{int}	0.0453	0.0216	0.0973	0.0644
Crystal size/ mm^3	0.30 × 0.23 × 0.07	0.50 × 0.40 × 0.35	0.31 × 0.19 × 0.15	0.25 × 0.13 × 0.05
Goodness-of-fit on F^2	1.031	1.077	0.937	1.093
$R_1[I>2\sigma(I)]$[a]	0.0521	0.0196	0.0367	0.0352
wR_2 (all data)[b]	0.1827	0.0524	0.1059	0.1228
Largest differences peak and hole (eÅ^{-3})	1.369 and -0.524	0.411 and -0.318	0.605 and -0.588	0.569 and -0.735

[a] $R_1 = \Sigma||F_o|-|F_c||/\Sigma|F_o|$. [b] $wR_2 = \{\Sigma[w(|F_o|^2-|F_c|^2)^2]/\Sigma[w(F_o^2)^2]\}^{1/2}$

View Article Online
DOI: 10.1039/C7NJ03551A

Results and Discussion

A controlled Mannich condensation between ethylenediamine, formaldehyde and 2,4–disubstituted phenols or 2−naphthol (1 : 2 : 2 molar ratio) in MeOH yields the corresponding secondary amine Mannich base ligands, H_2L^{1-5} in moderate to excellent yields. The reaction of the dibasic tetradentate Mannich base ligands, H_2L^{1-5} in 1:1 molar ratio with $[Mo^{VI}O_2(acac)_2]$ in MeOH, results in the formation of the corresponding dioxidomolybdenum(VI) complexes, $[Mo^{VI}O_2(L^{1-5})]$ (**1–5**) in good yields. All complexes are yellow/orange air stable solids, soluble in common organic solvents such as MeOH, $CHCl_3$, MeCN, DMSO, DMF etc.

Solid state characterizations

The coordination style of the ligands and the resulting geometry around the metal centre was confirmed by SC-XRD studies. ORTEP diagrams for the compounds $[MoO_2(L^1)]$ **1**, $[MoO_2L^2]$ **2**, $[MoO_2(L^3)]$ **3** and $[MoO_2(L^5)]$ **5** are presented in Figs. 1, 2, 3, and 4, respectively. Selected bond distances and angles are given in Table 2.

The structure of the complexes **1**, **2**, **3** and **5** adopt a distorted six-coordinated octahedral geometry with two O_{oxido} terminal oxygen atoms and the ligands act as tetradentate, coordinating through the two $O_{phenolate}$ and two N_{amine} atoms in a cis-α type binding mode involving coordination of one of the N_{amine} atom in the apical position and one O_{oxido} terminal oxygen atom in the equatorial position.[28] The axial sites are occupied by the oxido atoms, O(1), and by the nitrogen atoms, N(1), of the ligand. The equatorial plane is formed for the three atoms of the ligand [N(2), O(3) and O(4)] and one of the terminal oxygen atoms, O(2), and it is distorted with respect to the planarity, [mean deviation from the plane for N(2), O(2), O(3), O(4), 0.0041(2) Å in **1**, 0.0208(6) Å in **2**, 0.0298(11) Å in **3** and 0.0088(13) Å in **5**]. The molybdenum atoms are displaced toward the apical oxido ligand, O(1), from the equatorial plane defined by N(2), O(2), O(3) and O(4), 0.3025(3) Å in **1**, 0.3185(2) Å in **2**, 0.2712(12) Å in **3** and 0.2751(2) Å in **5**. The Mo-O_{oxido} bond lengths [Mo(1)-O(1) and Mo(1)-O(2) (see Table 2)] and bond angles [O=Mo=O angle are: 108.08(11)º in **1**, 108.93(6)º in **2**,106.67(11)º in **3** and 107.51(14)º in **5**] are within the ranges for the bond distances typically observed in these type of compounds.[29]

View Article Online
DOI: 10.1039/C7NJ03551A

π-π Interactions were not observed in the crystal packing of the four complexes. Intermolecular hydrogen bonds were observed in compounds **1**, **2** and **3** (see Table 3). Complex **2** forms self-assembled dimers in the solid state packing (Fig. 5), which are stabilized by C-H···π non covalent interactions in an antiparallel architecture. The distance between hydrogen atoms of the ethyl groups and centroids of the phenyl rings are 2.578 Å.[30] Interestingly, crystal packing of three complexes are entirely different while they belong to very similar ligand system (Figs. S1-S4).

Table 2 Bond lengths [Å] and angles [°] for $[MoO_2(L^1)]$ **1**, $[MoO_2L^2]$ **2**, $[MoO_2(L^3)]$ **3** and $[MoO_2(L^5)]$ **5**.

Bond lengths	**1**	**2**	**3**	**5**
Mo(1)-O(1)	1.710(2)	1.7055(10)	1.707(2)	1.708(2)
Mo(1)-O(2)	1.707(2)	1.7248(10)	1.701(2)	1.717(2)
Mo(1)-O(3)	1.939(2)	1.9460(10)	1.9364(18)	1.934(2)
Mo(1)-O(4)	1.936(2)	1.9546(9)	1.954(2)	1.965(2)
Mo(1)-N(1)	2.351(3)	2.3501(11)	2.345(2)	2.314(3)
Mo(1)-N(2)	2.356(3)	2.3077(11)	2.357(3)	2.316(3)
Angles	**1**	**2**	**3**	**5**
O(1)-Mo(1)-O(2)	108.23(12)	108.83(5)	106.67(11)	107.40(13)
O(1)-Mo(1)-O(4)	96.42(11)	96.13(4)	98.98(9)	97.21(10)
O(2)-Mo(1)-O(4)	97.42(11)	98.34(4)	95.58(8)	91.96(10)
O(1)-Mo(1)-O(3)	99.67(12)	98.76(5)	93.18(9)	96.02(11)
O(2)-Mo(1)-O(3)	93.78(11)	96.92(4)	99.61(8)	102.04(11)
O(4)-Mo(1)-O(3)	156.43(10)	153.94(4)	156.94(8)	156.88(10)
O(1)-Mo(1)-N(1)	160.52(11)	164.15(4)	163.31(10)	162.22(11)
O(2)-Mo(1)-N(1)	90.69(12)	86.63(4)	89.50(10)	90.37(12)
O(4)-Mo(1)-N(1)	75.99(10)	77.70(4)	83.15(8)	82.16(10)
O(3)-Mo(1)-N(1)	83.23(11)	82.26(4)	79.76(8)	79.47(10)

View Article Online
DOI: 10.1039/C7NJ03551A

O(1)-Mo(1)-N(2)	89.33(11)	90.98(5)	90.94(10)	89.18(11)
O(2)-Mo(1)-N(2)	161.92(11)	160.13(4)	162.35(10)	160.48(12)
O(4)-Mo(1)-N(2)	84.47(10)	80.45(4)	80.18(8)	75.55(10)
O(3)-Mo(1)-N(2)	78.64(10)	78.04(4)	80.11(8)	85.77(10)
N(1)-Mo(1)-N(2)	72.25(11)	73.69(4)	73.03(9)	73.31(10)

Table 3 Hydrogen bonds for [$MoO_2(L^1)$] **1**, [MoO_2L^2] **2** and [$MoO_2(L^3)$] **3**

Compound	D-H...A	d(D-H)	d(H...A)	d(D...A)	<(DHA)
1	N(2)-H(2N)...O(1)#1	0.95	2.31	3.067(4)	137.0
2	N(2)-H(2N)...O(2)#2	0.85(2)	2.06(2)	2.8663(14)	157.5(18)
3	N(1)-H(1N)...O(1)#3	0.96(3)	2.59(3)	3.194(3)	121(2)

Symmetry transformations used to generate equivalent atoms: #1 x-y,x,-z+1 #2 -x+1,y-1/2,-z+1/2 #3 x,y-1/2,-z+1/2

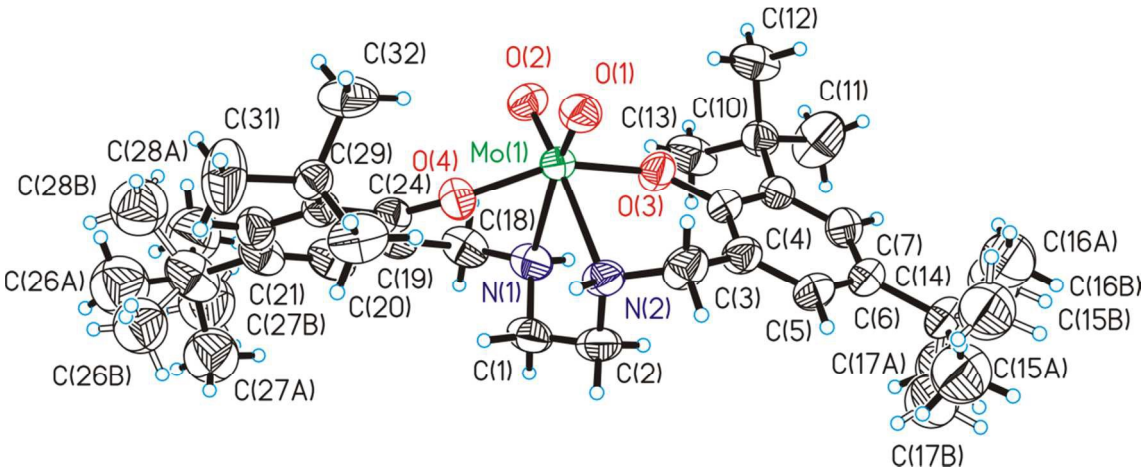

Fig. 1 ORTEP plot of complex [$MoO_2(L^1)$] **1**. All the non-hydrogen atoms are presented by their 50% probability ellipsoids.

View Article Online
DOI: 10.1039/C7NJ03551A

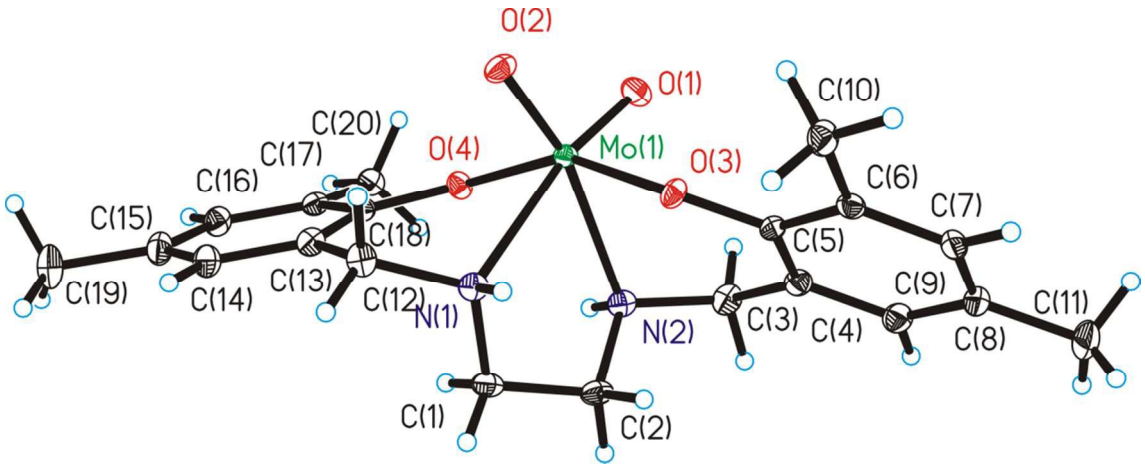

Fig. 2 ORTEP plot of complex [MoO_2L^2] **2**. All the non-hydrogen atoms are presented by their 50% probability ellipsoids.

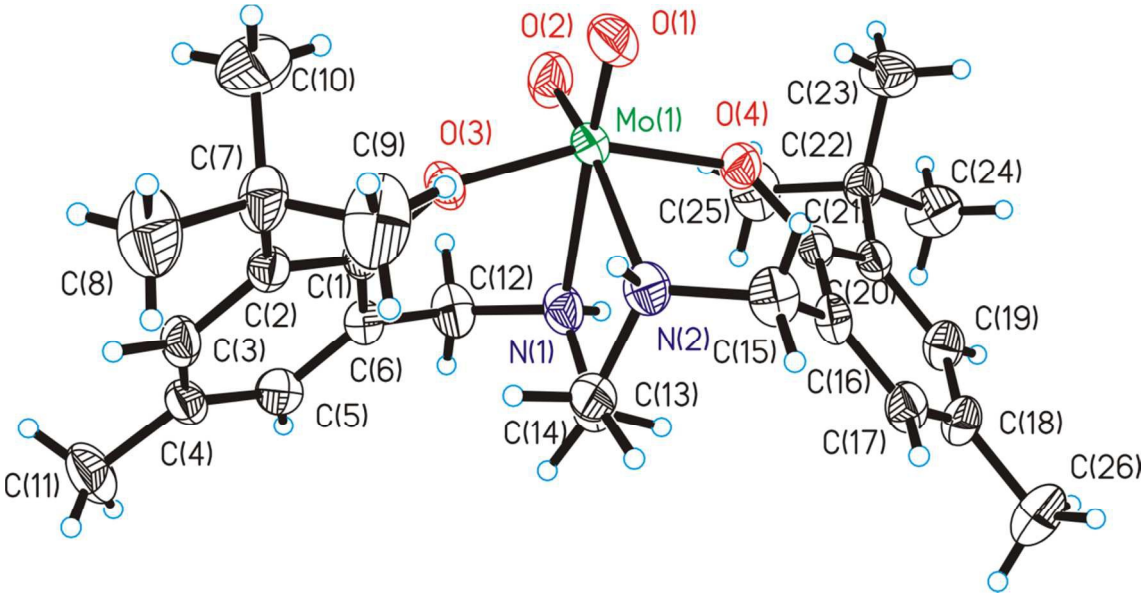

Fig. 3 ORTEP plot f complex [$MoO_2(L^3)$] **3**. All the non-hydrogen atoms are presented by their 50% probability ellipsoids.

View Article Online
DOI: 10.1039/C7NJ03551A

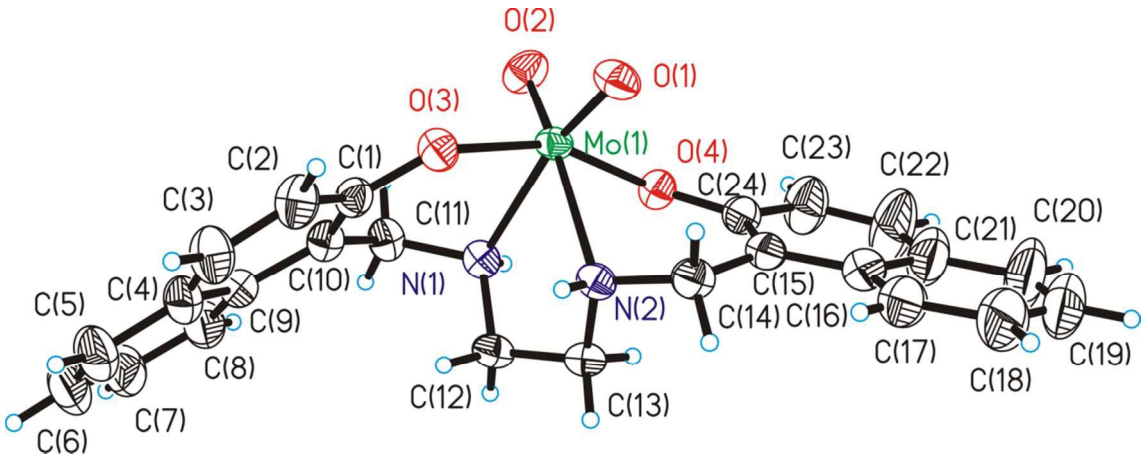

Fig. 4 ORTEP plot of complex $[MoO_2(L^5)]$ **5**. All the non-hydrogen atoms are presented by their 50% probability ellipsoids.

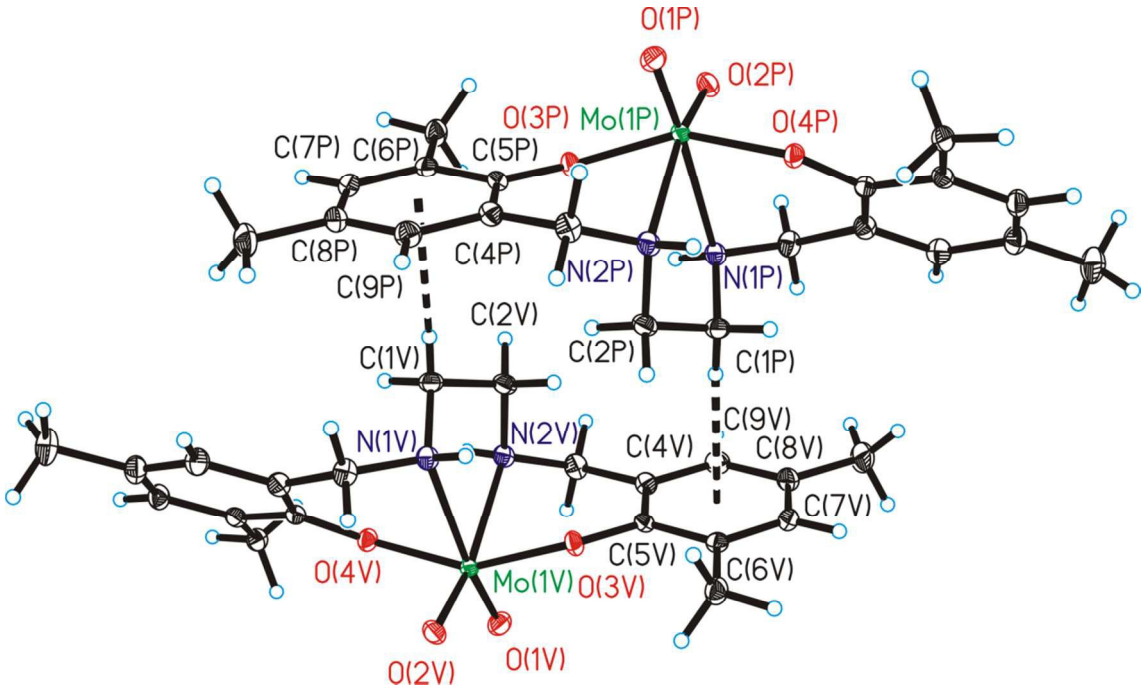

Fig. 5 X-ray fragment of $[MoO_2L^2]$ **2**. C-H···π interactions in **2** are present in the crystal packing and they are drawn in dashed black lines.

View Article Online
DOI: 10.1039/C7NJ03551A

Spectral Studies

The coordination modes of the ligands towards metal centre was further confirmed by spectroscopic analyses of all the ligands and the metal complexes. The IR spectra of all complexes exhibits two characteristics IR bands around 883-902 and 902-955 cm^{-1} (Table 4), due to the respective symmetric and asymmetric stretching of *cis*-[MoO_2] core.[31] Additionally, the broad peak around *ca.* 3400 cm^{-1} present in the spectra of all the ligands due to phenolic –OH is absent in the corresponding complexes indicating the coordination of phenolic oxygen following deprotonation. Coordination of nitrogen functionalities could not be ascertained unequivocally by IR spectral study because the spectra of the ligands as well as complexes both exhibit ν(NH) bands around 3050–3100 cm^{-1}. However, this coordination is well supported by single crystal X-ray study (vide supra). Other characteristic bands present in the spectra of the ligands as well as the complexes include the stretching frequencies around 2800–3000 cm^{-1} due to different alkyl substitution at the phenolic rings.

Table 4 Selected IR data (in cm^{-1}) for the ligands and complexes with tentative assignments.

Entry	Compounds	ν(OH)	ν(N-H)	ν_{asym}(O=Mo=O)	ν_{sym}(O=Mo=O)
1	H_2L^1, **I**	3270(b)	3000	-	-
2	[$Mo^{VI}O_2L^1$], **1**		2960, 3260	927	883
3	H_2L^2, **II**	3440(b)	3130(b)		
4	[$Mo^{VI}O_2L^2$], **2**		3182, 3295	927	884
5	H_2L^3, **III**	3425(b)	3050	-	-
6	[$Mo^{VI}O_2L^3$], **3**		3300	904	884
7	H_2L^4, **IV**	3440(b)	2990, 3128(b)		
8	[$Mo^{VI}O_2L^4$], **4**		3220	914	899
9	H_2L^5, **V**	3450(b)	3055	-	-
10	[$Mo^{VI}O_2L^5$], **5**		3055, 3245	955	902

View Article Online
DOI: 10.1039/C7NJ03551A

Table 5 presents UV/Vis spectral data of ligands and their *cis*–$[MoO_2]^{2+}$ complexes recorded in MeCN and Fig. 6 presents spectra of complexes. The UV-Vis spectra of the ligands display two spectral bands around 224–280 and 286–336 nm which can be attributed to $\pi\rightarrow\pi^*$ and $n\rightarrow\pi^*$ transitions, respectively (See Table 5 for exact values). These transitions undergo a hypsochromic shift in the metal complexes, and thus the corresponding UV-Vis spectra of the complexes display only the $n\rightarrow\pi^*$ band around 260–336 nm. This is possibly due to rearrangement of the ligand structure after coordination with metal ion. Additionally, all complexes also display an intense but broad band in the 330–380 nm due to ligand to metal charge transfer transition.

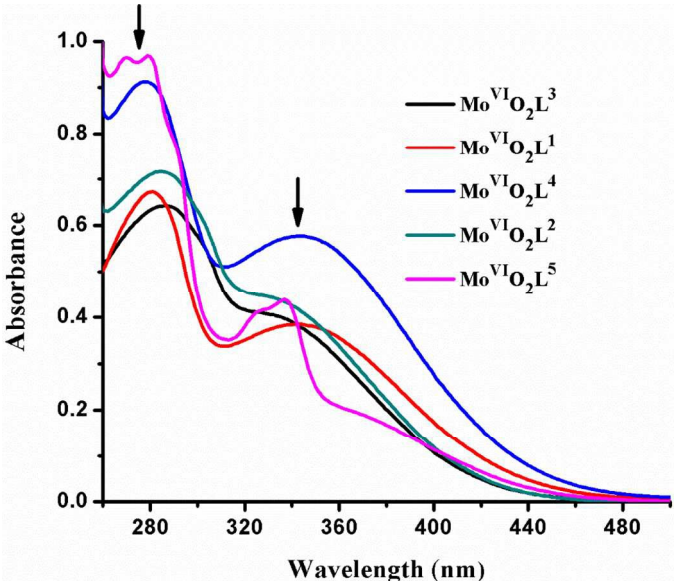

Fig. 6 UV/Vis spectra of complexes $[Mo^{VI}O_2L^{1-5}]$.

View Article Online
DOI: 10.1039/C7NJ03551A

Table 5 UV/Vis spectral data of ligands and complexes.

Compound	λ[nm] (ε, litre $mole^{-1}cm^{-1}$)
H_2L^1, **I**	234(2.48×10^3), 294(1.22×10^3)
$[Mo^{VI}O_2L^1]$, **1**	280(4.2×10^3), 345(2.39×10^3)
H_2L^2, **II**	224(1.46×10^3), 286 (4.73×10^3)
$[Mo^{VI}O_2L^2]$, **2**	284(3.25×10^3), 324(2.04×10^3)
H_2L^3, **III**	226(1.75×10^3), 286(1.02×10^3)
$[Mo^{VI}O_2L^3]$, **3**	285(3.46×10^3), 330(2.19×10^3)
H_2L^4, **IV**	237(1.43×10^3), 295(6.66×10^2)
$[Mo^{VI}O_2L^4]$, **4**	277(4.90×10^3), 342(3.09×10^3)
H_2L^5, **V**	280(2.23×10^3), 336(1.24×10^3)
$[Mo^{VI}O_2L^5]$, **5**	260(4.82×10^3), 336 (2.17×10^3), 380 (6×10^3)

The coordinating modes of ligands to the metal complexes were further ascertained by recording their ^{1}H NMR spectra in $CDCl_3$. Experimental section presents spectral data, Fig. 7 provides the representative spectra (ligand **II** and complex **2**) and Figs. S5 – S12 provide ^{1}H NMR spectra of other ligands and complexes for the series. All ligands' spectra show a signal at δ= 10.25–10.73 ppm due to two phenolic –OH protons which are equivalent in nature. The disappearance of this signal in the spectra of complexes indicates the coordination of the phenolic oxygen after their deprotonation. A relatively broad signal appearing at δ =3.45–3.64 ppm due to –NH protons in ligands shows slight shift in their position in the corresponding complexes, indicating their coordination to the metal center and the resulting change in electron density. Signals due to methylene groups, connecting to –NH and aromatic ring, appears as small singlet at δ =3.77-3.92 ppm except ligand H_2L^5 which exhibits two singlets at δ = 4.80 (s, 2H) and 4.3 (s, 2H) ppm.This signal become diastereotopic following coordination and splits into two doublets (in **2**, **4** and **5**) with two protons each or four doublets (in **1** and **3**) with one proton each and appear at relatively higher *δ* values. This trend is more common in tripodal ligand containing complexes.[32] Similarly, the ethylene protons attached to two dipodal –NH appears as singlet at δ =2.57-3.03 ppm in ligands and this splits into two triplets and appears at slightly lower positions. Signals due to aromatic protons, methyl and *tert*-butyl groups in ligands as well as in complexes appear in the expected region with slight variations.

View Article Online
DOI: 10.1039/C7NJ03551A

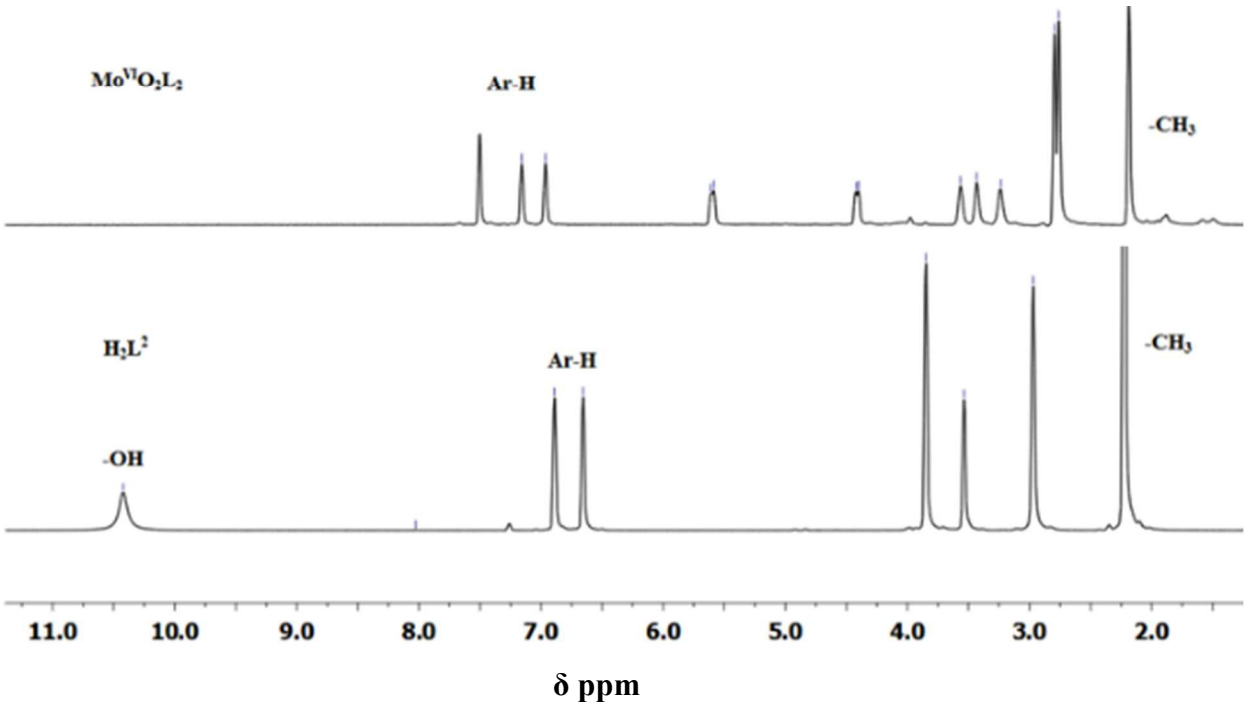

Fig. 7 ^{1}H NMR spectra of H_2L^2 and **2** in $CDCl_3$.

The binding modes of the ligands were further supported by the study of the coordination–induced ^{13}C NMR chemical shifts. The spectra were recorded in $CDCl_3$/DMSO-d_6 and the relevant data are presented in Table 6. All carbons resonate well within the expected regions; however, significant shifts, $\Delta\delta$ = [δ(complex) – δ(ligand)], were observed in the signals of the carbon atoms in the vicinity of the coordinating atoms. Thus, the carbons bearing the phenolic oxygens undergo a shift, $\Delta\delta$ between ~3.4 to -0.68 ppm (see Table 6). Similarly, the effect of coordination is also well pronounced on the ethylene protons, and they resonate with an average shift of $\Delta\delta$ between -11.48 to 7.99 ppm. A complete list of all peaks is included in the experimental section (see Fig. 8 as a representative).

View Article Online
DOI: 10.1039/C7NJ03551A

Table 6. ^{13}C NMR spectral data of ligands and complexes.

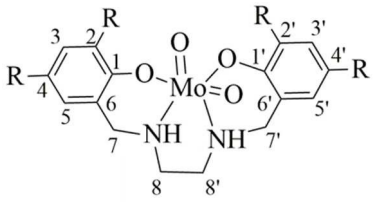

Compound [a]	C_1/C_1'	C_4/C_4'	C_7/C_7'	C8/C8′
H_2L^1	150.83	142.17	49.69	51.35
$[Mo^{VI}O_2L^1]$	154.23	140.84	51.87	59.34
(Δδ)	(3.4)	(2.03)	(2.18)	(7.99)
H_2L^2	153.13	131.24	58.36	51.77
$[Mo^{VI}O_2L^2]$	156.49	130.58	53.59	45.63
(Δδ)	(3.36)	(-0.66)	(-4.77)	(-11.48)
H_2L^3	154.21	136.07	58.05	50.89
$[Mo^{VI}O_2L^3]$	156.71	138.5	53.20	45.71
(Δδ)	(2.5)	(2.43)	(-4.85)	(-5.18)
H_2L^4	154.43	128.17	52.31	45.72
$[Mo^{VI}O_2L^4]$	153.75	127.40	50.20	45.97
(Δδ)	(-0.68)	(-0.77)	(-2.11)	(0.25)

[a] Δδ = [δ (complex) - δ (free ligand)].

View Article Online
DOI: 10.1039/C7NJ03551A

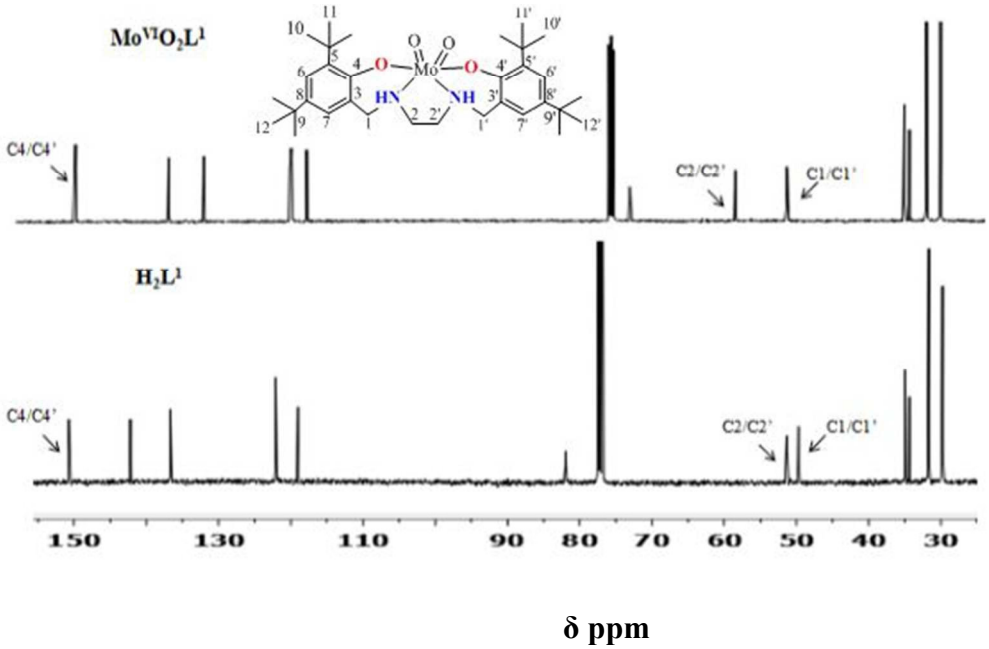

Fig. 8 ^{13}C NMR spectra [chemical shifts (δ) in ppm] of H_2L^3 and **3** in $CDCl_3$.

Oxygen atom transfer between benzoin and DMSO

Cis–dioxidomolybdenum(VI) complexes are known to catalyze oxygen atom transfer (OAT) in the presence of DMSO in a fashion similar to DMSO reductases. Most of these reactions reported in literature, are based on oxygen atom transfer between phosphines and/ or DMSO;[13-20] and only a few reports are available where OAT has been explored with a suitable organic substrate.[21-24] In our recent studies, we have reported the oxygen atom transfer ability of *cis*–dioxidomolybdenum(VI) complexes between DMSO and benzoin in acetonitrile at 80 ^oC. We have also proposed an overall steric control over the reaction mechanism, and identified suitable reaction intermediates.[21] The present study further explores the mechanistic details involving the oxygen atom transfer between DMSO and benzoin, catalyzed by *cis*–dioxidomolybdenum(VI) complexes. As the *cis*–dioxidomolybdenum (VI) complexes reported here are built on aminobisphenols, we have evaluated their electronic environment effect on OAT reactions between DMSO and benzoin in acetonitrile at 80 ^oC. The reaction was monitored over a period of 24 h, and the maximum conversion of 99 % to benzil selectively was achieved within 18 h at 80 ^oC using $[MoO_2L_5]$ **5** as a representative catalyst. The reaction was followed by

View Article Online
DOI: 10.1039/C7NJ03551A

measuring the decrease in the concentration of benzoin and formation of benzil via periodic HPLC analysis of the reaction mixture, eluted with water-acetonitrile-trifluoroacetic acid mixture (60:40:02) (Fig. 9).

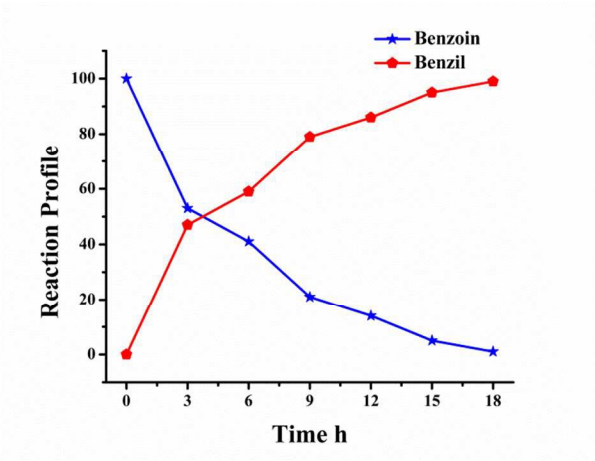

Fig. 9 The progress of the reaction as monitored by HPLC analysis of the reaction mixture at different time intervals using $[MoO_2(L^5)]$ **5** as the catalyst. Mobile phase: MeCN : H_2O : TFA 60 : 40 : 0.02 (for details, see text).

The reaction was initiated by taking benzoin (1.00 g, 5 mmol), DMSO (1 mL, 14 mmol) and the complex **5** as catalyst (3.00 mg, 6.02 µmol) in 10 mL of acetonitrile in a two neck 50 mL round bottom flask. DMSO was always taken in excess with respect to benzoin as well as the catalyst in all the reactions. The temperature of the reaction mixture was maintained at 80 ^oC for a period of 24 h, and the progress of the reaction was monitored by withdrawing small aliquots of the reaction mixture periodically and analyzing the same by HPLC analysis. A maximum of 99% conversion was achieved in 18 h and after that no further conversion was noted. Under the same reaction conditions, the other four complexes were also tested and the obtained results are collected in Table 7 and Fig. 10. Thus, the best conversion of 99 % was achieved by using 3.00 mg (6.02 µmol) of **5**.

View Article Online
DOI: 10.1039/C7NJ03551A

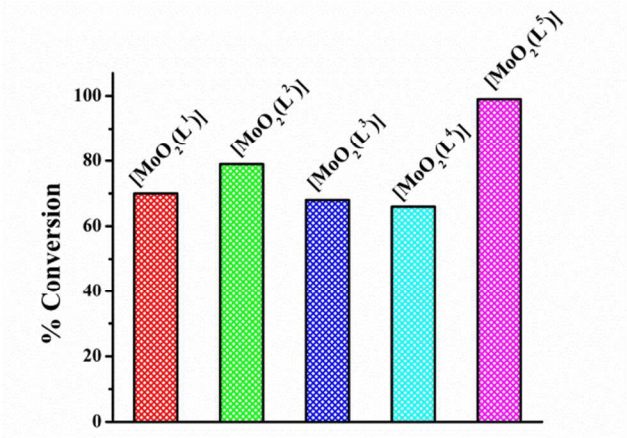

Fig. 10 Results for oxygen atom transfer reaction between DMSO and benzoin catalyzed by *cis*–$[MoO_2]^{2+}$complexes (for details, see text).

Table 7 Dioxidomolybdenum(VI) complexes catalyzed oxygen atom transfer between benzoin and DMSO in acetonitrile at 80 ^{o}C in 18 h of reaction time; conversion, TOF and selectivity data.

Entry	Catalyst	Catalyst [mg, µmol]	Conv.[%]	Selectivity [%]	TOF [h^{-1}]
1	$[Mo^{VI}O_2(L^1)]$ **1**	3.76, 6.02	70	100	33
2	$[Mo^{VI}O_2(L^2)]$ **2**	2.73, 6.02	79	100	37
3	$[Mo^{VI}O_2(L^3)]$ **3**	3.24, 6.02	68	100	31
4	$[Mo^{VI}O_2(L^4)]$ **4**	3.22, 6.02	66	100	31
5	$[Mo^{VI}O_2(L^5)]$ **5**	3.00, 6.02	99	100	46

The results of the catalytic OAT reaction between DMSO and benzoin using different catalysts, show a stark variation while changing the substituent on the phenol rings. Therefore, the complex with naphthyl rings, i.e. $[MoO_2(L^5)]$ **5** renders an excellent conversion of 99 %. This conversion drops to 70 – 80 % with alkyl substitution while the chloro substitution further slows down the reaction, and the overall conversion drops to 66 % in 18 h of reaction time for $[Mo^{VI}O_2(L^4)]$ **4**. These results can directly be correlated with the electronic environment of the *cis*–$[MoO_2]^{2+}$ core of the catalyst during the catalytic process and its consequences on the reaction mechanism. Most OAT reactions are thought to proceed via an associative mechanism;

View Article Online
DOI: 10.1039/C7NJ03551A

the reaction being initiated by the nucleophilic attack of the substrate (DMS in case of DMSO reductase) onto one of the more labile oxido groups of *cis*–$[MoO_2]^{2+}$moiety.[17,33,34] Thus, the substitutions on the ligands can affect the OAT reactions in two ways: (i) the electronic effect caused by the *para* substituent, and (ii) the steric effect caused by the *ortho* substituent. A bulky *ortho* substitution would hinder the approach of the incoming nucleophile, thus inhibiting the reaction. On the other hand, an electron donating *para* substitution would facilitate the nucleophilic attack of the substrate by compensating the electron density on the metal center because of the +I effect. Thus, when the *ortho* and *para* positions are substituted by chloro group, the reaction conversion drops to lowest, since the electron withdrawing chloro group exerts an –I effect, thus destabilizing the reaction intermediate. Consequently, complex **4** delivers the lowest conversion of 66 %. However, when the phenolic rings are replaced with naphthyl rings, the steric hindrance is reduced to minimal at the *ortho* positions, enabling an effective and strong interaction of the nucleophile with the metal center. Further, they also contribute towards stabilization of the reaction intermediate due to enhanced conjugation. Thus, the maximum conversion of 99 % is achieved with complex **5**. The results obtained with the other three catalysts are also in line with the *ortho* effects of alkyl substitution.[21] The Hammet plot also shows a good correlation for all the four electronic para substitutions (R^2= 0.98 and ρ = –1.78) (Fig. 11). This further substantiates our hypothesis of an electron deficient transition state during the reaction mechanism.

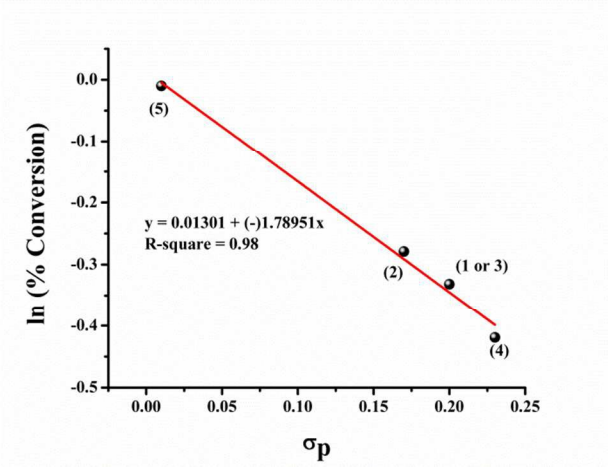

Fig. 11 Hammet plot for OAT reaction between DMSO and benzoin catalyzed by *cis*–$[MoO_2]^{2+}$ complexes.

View Article Online
DOI: 10.1039/C7NJ03551A

Dioxidomolybdenum(VI) complexes catalyzed oxygen atom transfer between 4-chlorobenzoin and DMSO have also been carried out in acetonitrile at 80 ^{o}C in 18 h of reaction time (Table S1 and Fig. S13). While 89-100% conversion was achieved with these complexes, the electron withdrawing chloro group again exerts an –I effect, destabilizing the reaction intermediate and consequently complex **4** gives the lowest conversion of 89 %.

We have performed a detailed kinetic analysis using the most active complex, **5** as the representative catalyst and deduced the rate equation for oxygen atom transfer between DMSO and benzoin. For this, a solution of **5** (3.00 mg, 6.02 μmol), benzoin (5 mmol) and DMSO (1 mL) in 10 mL MeCN was maintained at 80 ^{o}C. The reaction was performed for a period of 18 h and reaction mixture was analyzed as mentioned earlier.

The integrated rate equation for the OAT reaction between catalyst, benzoin and DMSO can be represented by equation 2. Since, the effective concentration of the catalyst does not change during the reaction, the reaction may be assumed to be following pseudo first order reaction kinetics. This was confirmed by the pseudo first order straight line plot obtained between log of decrease in concentration of benzoin *vs* time (Fig. 12). Equation 3 represents the resulting pseudo first order rate equation. The pseudo first order rate constant for **5** was found to be 0.0998 h^{-1}.

$$\text{Rate} = k_{obs}[\text{Benzoin}]^{x}[\text{Catalyst}]^{y} \quad (2)$$

$$\text{Rate} = k_{1}[\text{Benzoin}] \quad (3)$$

$$\text{where} \quad k_{1} = k_{obs}[\text{Catalyst}]^{y} \quad (4)$$

$$\ln k_{1} = \ln k_{obs} + y\ln[\text{Catalyst}] \quad (5)$$

View Article Online
DOI: 10.1039/C7NJ03551A

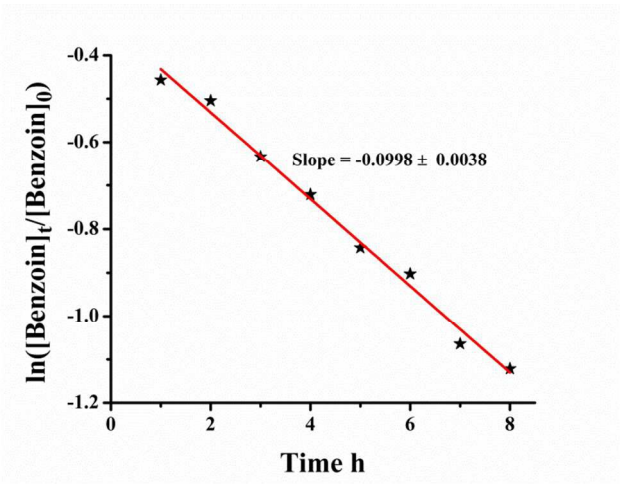

Fig. 12 Variation of [Benzoin] with time for the *cis*–[$Mo^{VI}O_2(L^5)$] **5** catalysed oxygen atom transfer reaction in the presence of DMSO. Reaction conditions: $[Benzoin]_0$ (5 mmol), DMSO (1.00 mL), catalyst (3.00 mg) and MeCN (10 mL).

The order of the reaction with respect to catalyst concentration was determined by solving equation 5, using the data inferred from Fig. 12. Thus, the rate of decrease in benzoin concentration after 18 h of reaction time at 80 ^oC in acetonitrile was monitored using different concentrations of the catalyst, [$Mo^{VI}O_2(L^5)$]. The relevant plot (lnk_1 *vs* ln[catalyst]) is shown in Fig. 13 and the observed order with respect to catalyst is found to be 0.94 and k_{obs} is 0.038 $M^{-1}h^{-1}$. Therefore, the overall rate equation may be represented as:

$$\text{Rate} = k_{obs}[\text{Benzoin}][\text{Catalyst}] \quad (6)$$
$$k_{obs} = 0.038\ M^{-1}\ h^{-1}$$

View Article Online
DOI: 10.1039/C7NJ03551A

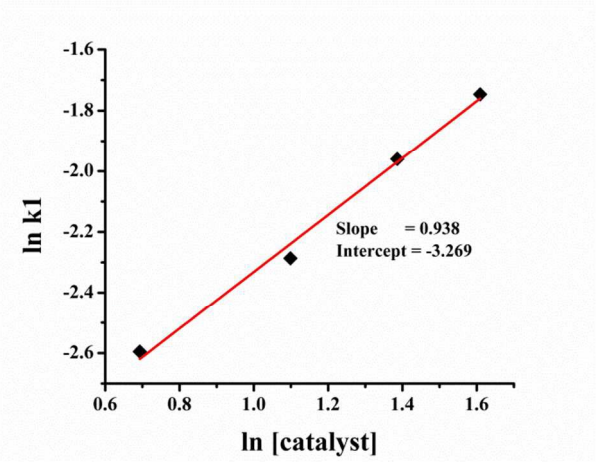

Fig. 13 Plot of $\ln k_1$ *vs* ln[catalyst] for oxido transfer reaction between benzoin and DMSO catalysed by $[Mo^{VI}O_2(L^5)]$ **5** at 80 ^oC for 18 h reaction time.

Most oxygen transfer reactions are thought to proceed via the formation of a Mo(V) dinuclear intermediate $[LMo^V–\mu–O–Mo^VL]$ (equations 7–8).[21] However, its formation is fast and reversible, and irreversible binuclear formation is often related to catalyst poisoning. During our studies, the formation of the binuclear intermediate and its fast decay into the initial dioxidomolybdenum(VI) complex was established by time dependent UV–Visible studies (Fig. 14). The reversible nature of the process is also authenticated by the fact that the order of the reaction in terms of catalyst was found to be unity.

View Article Online
DOI: 10.1039/C7NJ03551A

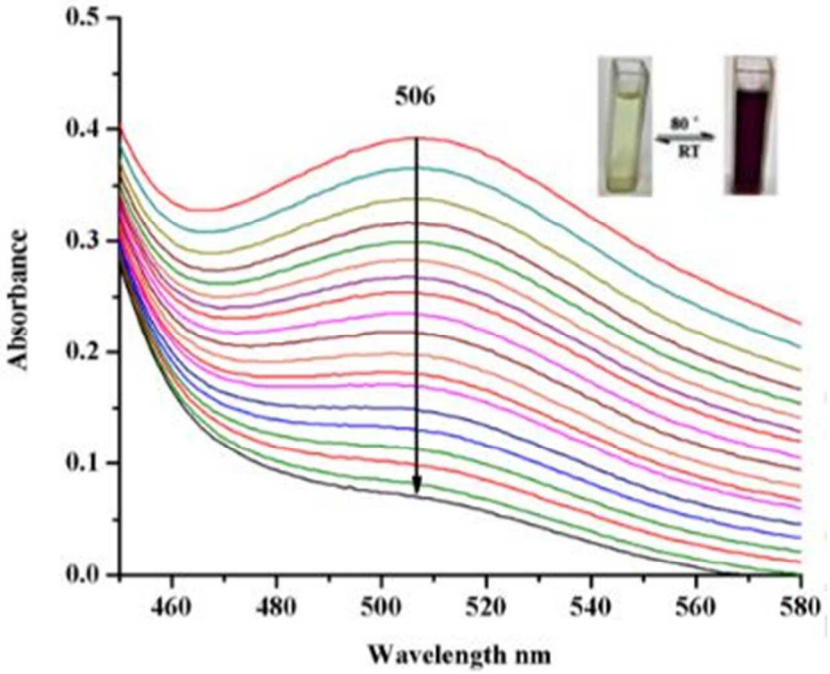

Fig. 14 Time-dependent spectral changes observed in the OAT reaction between **4**, benzoin and DMSO in acetonitrile after 8 h of reaction time. The spectra were recorded every 10 s from 80 ^{o}C to room temperature.

$$[Mo^{VI}O_2(L^n)] + DMS \rightleftharpoons [Mo^{IV}O(L^n)] + DMSO \quad (7)$$

$$[Mo^{VI}O_2(L^n)] + [Mo^{IV}O(L^n)] \rightleftharpoons [L^nMo^{V}(=O)-O-(O=)Mo^{V}L^n] \quad (8)$$

Conclusions

Five dibasic tetradentate ONNO donor Mannich bases H_2L^{1-5} derived from ethylenediamine and 2,4–di–*tert*–butylphenol, 2,4–di–methylphenol, 2–*tert*–butyl–4–methylphenol, 2,4–di–chlorophenol and 2-naphthol and their corresponding *cis*-MoO_2 complexes, $[Mo^{VI}O_2(L^{1-5})]$ have been isolated and characterized. The isolated complexes have successfully been used as catalysts for oxygen atom transfer between benzoin or 4-chlorobenzoin and dimethyl sulfoxide (DMSO) in acetonitrile at 80 °C, similar to DMSO reductase. As high as 100% conversion, monitored by HPLC was achieved with complex **5**. The electron withdrawing chloro group exerts an –I effect, destabilizing the reaction intermediate and consequently complex **4** gives the lowest conversion

View Article Online
DOI: 10.1039/C7NJ03551A

of 66% for benzoin and 89% for 4-chlorobenzoin. The naphthyl ring reduces the steric hindrance at the *ortho* position, stabilizing the reaction intermediate due to enhanced conjugation and consequently complex **5** gives highest conversion. Other substituents have intermediate effect. The Hammet plot also presents a good correlation for all the four para substitutions (R^2= 0.98 and ρ = –1.78). A detail kinetic study supports the pseudo first order reaction; the obtained pseudo first order rate constant for **5** is 0.0998 h^{-1}. UV/Vis spectroscopy suggested the plausible formation of the binuclear intermediate [LMo^{V}–μ-O–$Mo^{V}L$] during catalytic action and its fast decay to the initially taken monomeric complex.

Conflicts of Interest

There are no conflicts of interest to declare.

Acknowledgments

M. R. M. thanks the Science and Engineering Research Board (SERB), Department of Science and Technology, Government of India, New Delhi for financial support of the work (grant number EMR/2014/000529). B. M. is thankful to the Indian Institute of Technology Roorkee for an MHRD fellowship.

References

1 (*a*) A. Majumdar and S. Sarkar, *Coord. Chem. Rev*., 2011, **255**, 1039–1054; (*b*) G. Dong and U. Ryde, *J. Inorg. Biochem*., 2017, **171**, 45–51.

2 (*a*) R. Hille, T. Nishino and F. Bittner, *Coord. Chem. Rev*., 2011, **255**, 1179–1205; (*b*) A. Thapper, A. Behrens, J. Fryxelius, M. H. Johansson, F. Prestopino, M. Czaun, D. Rehder and E. Nordlander, *Dalton Trans*., 2005, 3566–3571; (*c*) R. Hille, *Chem. Rev*., 1996, **96**, 2757–2816; (d) R. Hille, *Trends Biochem. Sci*., 2002, **27**, 360–367.

3 D. C. Rees, Y. Hu, C. Kisker and H. Schindelin, *J. Chem. Soc., Dalton Trans*., 1997, 3909–3914.

4 R. Hille, *Dalton Trans*., 2013, **42**, 3029–3042.

5 P. V. Bernhardt, Ed. Jason Davis, Royal Society of Chemistry, 2009, pp.1–24.

View Article Online
DOI: 10.1039/C7NJ03551A

6 (*a*) P. V. Bernhardt, *Chem. Commun*., 2011, **47**, 1663–1673; (*b*) M. J. Romão, *Dalton Trans*., 2009, 4053–4068.

7 M. J. Pushie, J. J. Cotelesage and G. N. George, *Metallomics*, 2014, ***6***, 15–24.

8 X. Ma, C. Schulzke, H. G. Schmidt and M. Noltemeyer, *Dalton Trans*., 2007, 1773–1780.

9 A. Majumdar, *Dalton Trans.,* 2014, **43**, 8990–9003.

10 T. Paul, P. M. Rodehutskors, J. Schmidt and N. Burzlaff, *Eur. J. Inorg. Chem*., 2016, 2595–2602.

11 H. Sugimoto, M. Sato, K. Asano, T. Suzuki, K. Mieda, T. Ogura, T. Matsumoto, L. J. Giles, A. Pokhrel, M. L. Kirk and S. Itoh, *Inorg. Chem*., 2016, **55**, 1542–1550.

12 J. T. Hoffman, S. Einwaechter, B. S. Chohan, P. Basu and C. J. Carrano, *Inorg. Chem*., 2004, **43**, 7573–7575.

13 A. Ducrot, B. Scattergood, B. Coulson, R. N. Perutz and A. K. Duhme-Klair, *Eur. J. Inorg. Chem*., 2015, 3562–3571.

14 C. J. Whiteoak, G. J. P. Britovsek, V. C. Gibson and A. J. P. White, *Dalton Trans*., 2009, 2337–2344.

15 P. Basu, B. W. Kail, A. K. Adams and V. N. Nemykin, *Dalton Trans*., 2013, **42**, 3071–3081.

16 R. Dinda, P. Sengupta, S. Ghosh and W. S. Sheldrick, *Eur. J. Inorg. Chem*., 2003, 363–369.

17 G. Lyashenko, G. Saischek, M. E. Judmaier, M. Volpe, J. Baumgartner, F. Belaj, V. Jancik, R. H. Irmerd and N. C. Mösch-Zanetti, *Dalton Trans*., 2009, 5655–5665.

18 M. E. Judmaier, A. Wallner, G. N. Stipicic, K. Kirchner, J. Baumgartner, F. Belaj and N. C. Mösch-Zanetti, *Inorg. Chem*., 2009, **48**, 10211–10221.

19 X. Ma, C. Schulzke, Z. Yang, A. Ringe and J. Magull, *Polyhedron*, 2007, **26**, 5497–5505.

20 C. E. A. Andrade, X. Ma, W. Meyer-Klaucke and C. Schulzke, *Polyhedron*, 2010, **29**, 664–668.

21 M. R. Maurya, B. Uprety and F. Avecilla, *Eur. J. Inorg. Chem*., 2016, 4802–4813.

22 Y. L. Wong, Y. Yan, E. S. H. Chan, Q. Yang, T. C. W. Mak and D. K. P. Ng, *J. Chem. Soc., Dalton Trans.,* 1998, 3057–3064.

23 Y. L. Wong, Q. Yang, Z. Y. Zhou, H. K. Lee, T. C. W. Mak and D. K. P. Ng, *New J. Chem*., 2001, **25**, 353–357.

View Article Online
DOI: 10.1039/C7NJ03551A

24 A. Lehtonen and R. Sillanpää, *Polyhedron*, 2005, **24**, 257–265.

25 G. J. J. Chen, J. W. McDonald and W. E. Newton, *Inorg. Chem*., 1976, **15**, 2612–2615.

26 G. M. Sheldrick, *SADABS*, version 2.10, University of Göttingen, Germany, 2004.

27 G. M. Sheldrick, *Acta Crystallogr. Sect. C*, 2015, **71**, 3–8.

28 P. Adão, M. R. Maurya, U. Kumar, F. Avecilla, R. T. Henriques, M. L. Kusnetsov, J. Costa Pessoa and I. Correia, *Pure Appl. Chem*., 2009, **81**, 1279–1296.

29 N. K. Ngan, K. M. Lo and C. S. R. Wong, *Polyhedron*, 2011, **30**, 2922–2932.

30 S. Thakur, S. Roy, A. Bauzá, A. Frontera, S. Chattopadhyay, *Inorg. Chim. Acta*, 2017, **467** 212–220.

31 A. Syamal and M.R. Maurya, *Coord. Chem. Rev.*, 1989, **95**, 183-238.

32 (*a*) M. R. Maurya, B. Uprety, F. Avecilla, P. Adao and J. Costa Pessoa, *Dalton Trans.*, 2015, **44**, 17736–17755; (*b*) T. Heikkila, R. Sillanpää and A. Lehtonen, *J. Coord. Chem.*, 2014, **67**, 1863–1872; (*c*) Y. L. Wong, L. H. Tong, J. R. Dilworth, D. K. P. Ng and H. K. Lee, *Dalton Trans.*, 2010, **39**, 4602–4611; (*d*) F. Wolff, C. Lorber, R. Choukroun and B. Donnadieu, *Inorg. Chem*., 2003, **42**, 7839–7845.

33 J. H. Enemark, J. J. A. Cooney, J. J. Wang and R. H. Holm, *Chem. Rev*., 2004, **104**, 1175–1200.

34 P. Basu, B. W. Kail and C. G. Young, *Inorg. Chem*., 2010, **49**, 4895–4900.

View Article Online
DOI: 10.1039/C7NJ03551A

((Table of contents))

Oxygen atom transfer between DMSO and Benzoin catalyzed by *cis*–dioxidomolybdenum(VI) complexes of tetradentate Mannich bases.

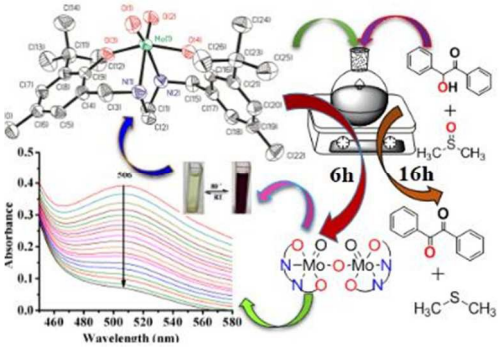

***Cis*–$[MoO_2]^+$ Complexes**

M. R. Maurya,*B. Mengesha, B. Uprety, N. Jangra, Reshu, F. Avecilla,

Dioxidomolybdenum(VI) complexes of tetradentate ONNO donor Mannich base ligands for the catalytic oxygen atom transfer between benzoin and DMSO are reported.

Keywords: Molybdenum complexes / crystal structure/ DMSO Reductases/ NMR spectroscopy / Oxygen atom transfer